An Estimate of Interference Effect From the Los Angeles Area High-Density Fixed Services (HDFS) on the Goldstone DSN Receiver Above 30 GHz: Monte Carlo Simulation

C. Ho,[1] M. Sue,[1] and C. Ruggier[1]

A large number of microwave transmitters will be installed in large urban centers in the future to provide high-density fixed services (HDFS). The frequency band proposed for use by these transmitters overlaps the Ka-band (27–40 GHz) allocated for NASA's Deep Space Network (DSN) receivers. Interference signals from these transmitters can propagate over the horizon and interfere with the DSN through various mechanisms, such as ducting, rain scattering, and diffraction. In this article, we have used the available International Telecommunication Union (ITU) models and a Monte Carlo simulation to estimate the aggregate interference power from the HDFS transmitters in the Los Angeles area as received by a DSN station located at Goldstone, California. It was found that, for a worst-case scenario, when a single transmitter main beam points to the DSN antenna and the separation distance is less than 200 km, the threshold for protecting the DSN receiver at Ka-band will be exceeded. An urban area such as Los Angeles has been assumed to have 3000 HDFS transmitters spreading with various maximum radial distances. Our simulation shows that the distributed effective isotropic radiated power (EIRP) of multiple HDFS sites will produce higher interference power at Goldstone as compared with an equivalent single transmitter with a normally distributed EIRP. When the HDFS spatial distribution has a maximum radial distance of 50 km, the received interference power at Goldstone exceeds the DSN threshold. The aggregate power and antenna gain increase with increasing transmitter numbers and distributed radial distances. This article provides solid results for consideration by the ITU and the HDFS community, and presents possible interference-mitigating approaches for the future HDFS deployment.

I. Introduction

Commercial operators are now proposing to install hundreds and thousands of high-density fixed services (HDFS) microwave transmitters in large urban centers [1] such as Los Angeles. These transmitters will share the same frequencies in the Ka-band (32 GHz and 37 to 38 GHz) with some Space

[1] Communication Systems and Research Section.

Research Service (SRS) receiving Earth stations. To face this challenge, the World Radio Communications Conference-97 (WRC-97) Resolution 126 requested that the International Telecommunication Union–Radio Communication (ITU-R) conduct, as a matter of urgency and in time for the World Radio Communications Conference-99 (WRC-99), appropriate studies to determine sharing criteria between stations in the fixed service and stations in other services that are allocated the same frequencies [2]. The three DSN worldwide tracking stations utilize this frequency band and may become vulnerable to interference from the planned deployment of HDFS transmitters. Since these HDFS transmitters operate at relatively strong signal power (up to −60 dBW/Hz), they will seriously interfere with the sensitive DSN receivers. Thus, it has become imperative to accurately predict the impact of HDFS transmitters on NASA's DSN receivers in the Ka-band.

The procedures for calculating the coordination distances around an SRS Earth station for interference from a point-to-point transmitter, such as in ITU-R Recommendations IS.847, P.620, and P.452, have been well documented [1,3–8]. The procedures in these recommendations are based on the computation of the minimum permissible transmission loss that satisfies the protection criteria for emissions originating at a single station [3–7]. These conditions do not apply to a high-density deployment with multiple terrestrial transmitters over an extended area. Recently, ITU–Joint Rapporteurs Group (ITU-JRG) 7D/9D [9–12] developed a method to theoretically calculate the aggregate gain from a large number of HDFS transmitters by using a normal distribution. They assumed that HDFS transmitter sites will not be spatially distributed, which differs significantly from a real HDFS deployment pattern. Thus, this method may underestimate the interference effects, since multiple HDFS transmitters were considered to be equivalent to a single transmitter with an aggregate net power. To simulate a real transmitter distribution, we need to examine the integrated interference power from a large number of HDFS transmitters with various spatial distributions. In this article, we followed a Monte Carlo approach to simulate several thousand HDFS transmitter sites spreading in the Los Angeles area and to calculate the interference power received at the Goldstone, California, tracking station. Models and procedures that were used are described in the following section.

II. Models and Procedures

There are several mechanisms [3,5–7,13–15] that can cause the interference signals to propagate with significantly low attenuation, as shown in Fig. 1. Other than direct coupling within a line of sight between the receiving Earth station and the transmitter, interference signals also can propagate over the horizon through diffraction, surface or elevated ducting, rain scattering, the tropospheric scatter mechanism, etc. [3,5–7]. The diffraction propagation mechanism only makes a contribution at relatively short distances (<200 km) [16], while coupling through rain scattering becomes less effective beyond the 300-km range [17,18]. Ducting-propagation effects, however, remain important over a wider range (∼500 km) [19,20]. Interference by tropospheric scatter is generally too low to be considered in this article [13,14].

A. Path Profile Analysis

At first, the profile for the interference-signal propagation path was analyzed to identify which interference mechanisms are related to geomorphologic features [3]. Because the main purpose of this article is to assess interference effects from transmitters in the Los Angeles area on the Goldstone DSN receiver, a simplified topographic map for this area is presented in Fig. 2. The center of Los Angeles is about 200 km away from Goldstone. Along the great circle path between the two locations, there are four major mountain peaks. Two mountain peaks within the San Gabriel Mountains have greater heights (1900 m and 2750 m), which will cause large diffraction losses and partially block the surface-ducting propagation. However, interference signals still can propagate to the Goldstone site through an elevated duct and rain scattering. Four small cities behind the San Gabriel Mountains will have lower diffraction losses since there are no large mountain peaks that block the surface propagation toward the Goldstone antenna.

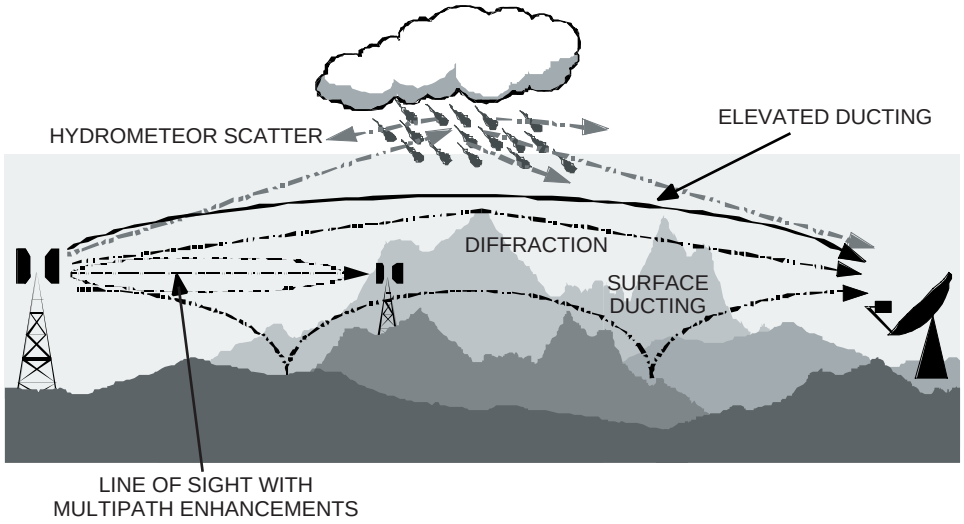

Fig. 1. Four types of interference propagation mechanisms: line of sight, diffraction, surface and elevated ducting, and rain scattering. Ducting and rain scattering are two dominant effects that can interfere with a transhorizon receiver.

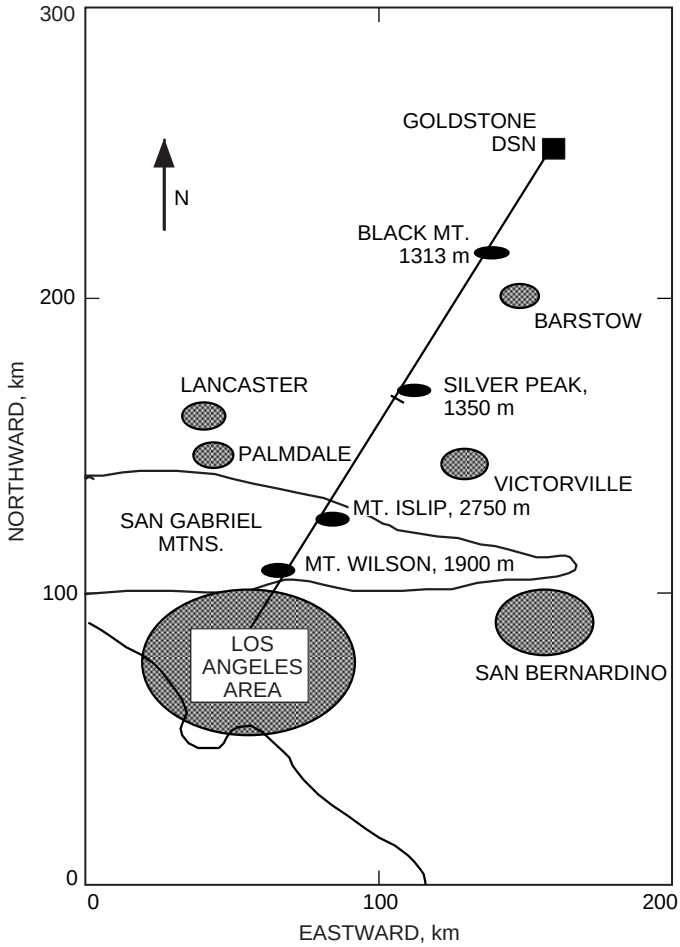

Fig. 2. A simplified topographic profile between Los Angeles and the Goldstone DSN receiver site. There are four major mountain peaks in the path. Urban areas in Los Angeles and other nearby cities also are shown.

B. HDFS Power Distribution

Three types of HDFS transmitters have been planned by the fixed service: point-to-point, point-to-multipoint (user terminals), and point-to-multipoint (hub terminals). According to the proposed HDFS data [1], each type of transmitter has a different power range and distribution. Among the three types of transmitters, point-to-point transmitters have the highest power and are the only type considered in this article. The percentage of power distribution for this type of transmitter is listed in Table 1. The point-to-multipoint transmitters were not considered in this simulation since they will operate at lower EIRP levels than will the point-to-point transmitters (worst-case interference).

The total transmitter deployment numbers depend on the area of the urban population centers. Generally, one point-to-point transmitter can cover 5 km^2. Based on this density, in the Los Angeles metropolitan area (15,000 km^2), it is expected that about 3000 transmitters will be distributed randomly.

Table 1. Point-to-point transmitter power distribution.

Percent of transmitters	Power output range P_r, dBW/Hz
15	$P_r \le -85$
18	$-85 < P_r \le -80$
27	$-80 < P_r \le -75$
18	$-75 < P_r \le -70$
18	$-70 < P_r \le -65$
4	$-65 < P_r \le -60$

C. HDFS Transmitter Antenna Model

All point-to-point transmitters were assumed to be horizontally pointed (elevation angle $\theta = 0$ deg). The typical point-to-point transmitter antenna-gain pattern has a pencil beam. Its gain (G_t, in dB) pattern is documented in ITU-R F.1245 [21] as a function of azimuthal angle (φ):

$$\left.\begin{aligned} G_t(\varphi) &= 46 - 2.5 \times 10^{-3} \left(\frac{D}{\lambda}\varphi\right)^2 && \text{for } 0 \text{ deg} \le \varphi < \varphi_m \\ G_t(\varphi) &= 29 - 25 \log \varphi && \text{for } \varphi_m \le \varphi < 48 \text{ deg} \\ G_t(\varphi) &= -13 && \text{for } 48 \text{ deg} \le \varphi \le 180 \text{ deg} \end{aligned}\right\} \quad (1)$$

where D is the antenna diameter (0.8 m), λ is the wavelength for a 32-GHz wave (0.0094 m), and φ_m is the first side-lobe angle (1.4 deg). Thus, for a transmitter with a main-lobe gain of 46 dB, the maximum EIRP is $P_t + G_t = -60$ dBW/Hz + 46 dB = -14 dBW/Hz.

D. Transmission Loss Models [3,6,7]

On the basis of ITU models, the line-of-sight, diffraction, ducting, and rain-scattering losses are discussed in the following subsections.

1. Line of Sight (Free Space Loss). For a line-of-sight propagation, the received power, P_r, is defined as

$$P_r = \frac{P_t G_t G_r}{L_b} = \frac{P_t G_t G_r}{L_{fs} L} \tag{2}$$

where $L_b = L_{fs}L = (P_t G_t G_r)/P_r$ is the basic transmission loss, $L_{fs} = ([4\pi df]/c)^2$ is the free space loss, d is the distance between the receiver and transmitter, c is the speed of light, P_t is the transmitter power, and G_r is the receiver antenna gain. Thus, there is a general relation in logarithm:

$$P_r = EIRP + G_r - L_b \tag{3}$$

in dB. Furthermore,

$$L_{fs} = 20\left[\log\left(\frac{4\pi}{c}\right) + \log f + \log d\right] \tag{4}$$

in dB. Changing units of frequency, f, from Hz to GHz, and of d from m to km, we have

$$L_{fs} = 92.45 + 20\log f + 20\log d \tag{5}$$

in dB. In Eq. (2), L is the correction term for loss:

$$L = A_g + A_d \tag{6}$$

in dB, where A_g is gaseous attenuation [22], A_d is the defocus factor due to the Earth's curvature, and

$$A_g = (\gamma_o + \gamma_w)d = 0.2d \tag{7}$$

where γ_o is loss from oxygen and γ_w is loss from water vapor, in dB/km. Thus,

$$L_b - L_{fs} + L = L_{fs} + A_g + A_d \tag{8}$$

in dB. When $f = 32$ GHz and $d = 200$ km, we have $L_b = 188$ dB.

2. Diffraction Over Mountains [16]. Diffraction loss, L_d, is defined as

$$L_d = L_b + L_{ds} = L_b + \sum_i J_i(\nu) \tag{9}$$

in dB, where $L_{ds} = \sum_i J_i(\nu)$ is all subpath diffraction over edges and troughs in the path profiles and $J(\nu)$ is a function defined in [16]. For a 200-km path profile between Los Angeles and Goldstone, there are four major mountain peaks. The total subpath diffraction loss is

$$\sum_i K_i(\nu) = 33$$

in dB. Thus, total loss due to diffraction is 221 dB over a 200-km path from Los Angeles to Goldstone.

3. Transhorizon Ducting (Mode 1) [3,5–7,13,14]. For a transhorizon ducting propagation along the great circle of the Earth, the transmission loss, L_1, is a function of p, the percentage of time of a weather condition:

$$L_1(p) = 92.5 + 20\log f + 10\log d_1 + A_h + [\gamma_d(p) + \gamma_o + \gamma_w]d_1 \tag{10}$$

in dB. Different from a two-dimensional free space loss, $20\log d$, given in Eq. (5), ducting propagation has a one-dimensional loss, $10\log d_1$, due to tropospheric layer trapment. In Eq. (10), $A_h = 7.5$ dB is a loss due to ducting coupling and obstacles, and $\gamma_d(p)$ is ducting attenuation (0.1954 dB/km), a function of the percentage of time. Taking an approximation of $10\log d_1 = 20 + 0.01d_1$, and $\gamma(p) = 0.01 + \gamma_d(p) + \gamma_o + \gamma_w$, we have

$$L_1(p) = 120 + 20\log f + \gamma(p)d_1 + A_h \tag{11}$$

in dB.

Transmission loss for ducting as a function of required time percentage for which the loss is not exceeded is plotted in Fig. 3 for different distances and for $p = 0.001$, $d_1 = 200$ km, and $\gamma_d d_1 = 38$ dB. Thus,

$$L_1(0.001) = 208$$

in dB. Corresponding to a larger p, there is a larger loss, L_1, or smaller interference. Similarly to Eq. (3), the received interference power is given by

$$P_r(p) = EIRP + G_r - L_1(p) \tag{12}$$

in dB.

4. Rain Scattering (Mode 2) [3,6,7,17,18,23]. For the rain-scattering transmission loss, L_2, a definition different from that for ducting loss is used. The received interference power is independent of receiver antenna gain:

$$L_2(p) = \frac{P_t}{P_r} \tag{13}$$

From the radar equation, we have

$$P_r = \frac{P_t G_r \eta V A_r}{(4\pi)^2 (R_1)^2 (R_2)^2} \tag{14}$$

where η is the cross-section/unit volume, A_r is the effective receiver antenna area, V is the scattering volume, and R_1 and R_2 are distances (km) from rain cells to the transmitter and the receiver, respectively. Transmission loss due to the rain scattering is [6]

$$L_2(p) = 168 + 20\log d_2 - 20\log f - 13.2\log R - G_t + 10\log A_b - 10\log C + \Gamma + \gamma_g d_2 \tag{15}$$

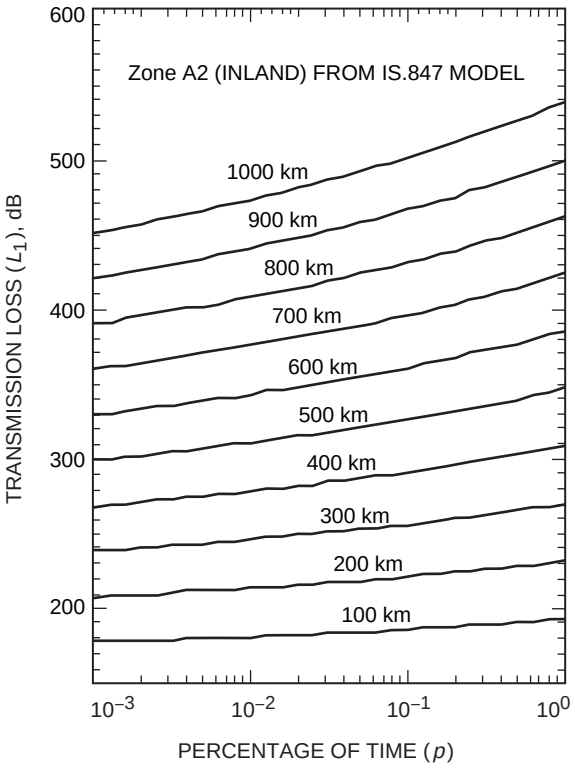

Fig. 3. Transmission loss due to ducting along a great circle as a function of the percentage of time in weather exceeded, for distances from 100 to 1000 km.

in dB, where R is the rain rate, a function of percentage of time of the weather condition, A_b, and C and Γ are other correction factors. The loss as a function of p, the percentage of time in weather exceeded, is plotted in Fig. 4 for different distances. For $p = 0.001$ in rain zone E, a 200-km distance, and a transmitter gain of $G_t = 46$ dB, we have $L_2 = 160$ dB.

Furthermore, we also can represent the loss in another form, because

$$\begin{aligned} P_r(p) &= P_t - L_2(p) = P_t + G_t - L_2(p) - G_t \\ &= EIRP - [L_2(p) + G_t] \\ &= EIRP - L_2^*(p) \end{aligned} \tag{16}$$

in dB. Thus, $L_2^*(p) = L_2(p) + G_t = 206$ dB. This value is close to the ducting transmission loss over 200 km for a 0.001 probability. As a comparison, L_1, L_2, and L_2^* are plotted in Fig. 5.

To summarize, for a single transmitter with a distance, d, of 200 km; a frequency, f, of 32 GHz; and time percent, p, of 0.001 percent, we have

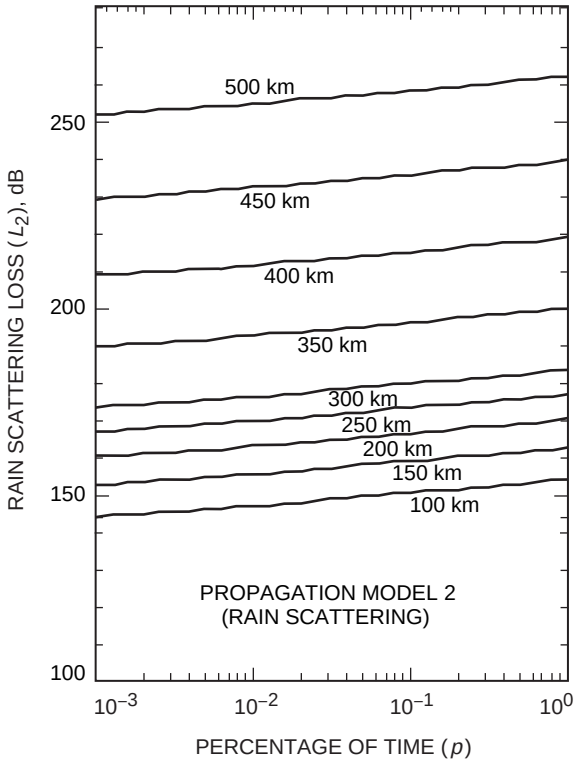

Fig. 4. Transmission loss due to rain scattering as a function of the percentage of time in weather exceeded, for distances from 100 to 500 km.

$L_b =$ 188 dB (line-of-sight loss, including gaseous attenuation)

$L_d =$ 221 dB (diffraction loss over mountains)

$L_1 =$ 208 dB (ducting transmission loss, 0.001 percent of the time)

$L_2^* =$ 206 dB (rain-scattering loss, 0.001 percent of the time)

Through this comparison, we find that both ducting and rain scattering have smaller transhorizon losses and, thus, cause stronger coupling of the interference signals. The simulation was performed to determine interference coupling in the ducting mode only.

5. DSN Receiver Model [24]. There are three NASA DSN receivers, which are located in Goldstone, California, USA; Canberra, Australia; and Madrid, Spain, respectively. In this article, only the Goldstone 70-m receiver antenna was modeled. DSN operations allow the interference to be exceeded by 0.001 percent of the time (weather condition) in order to meet the requirement for manned space missions. This receiver antenna has a gain (pencil-beam) pattern similar to that of a point-to-point transmitter antenna, as described in Subsection II.C [21]. Here we have used a standard large antenna model as documented in ITU Radio Regulations [24] for a DSN antenna pattern with the following parameters: a DSN antenna with a diameter of $D = 70$ m; a threshold power spectral flux density of $p_d = -251$ dBW/m^{2}Hz at Ka-band; and a corresponding threshold power spectral density of $P_{th} = \zeta\pi(D/2)^2 p_d = -217$ dBW/Hz, where antenna efficiency, ζ, is 52 percent, main-lobe gain at the bore site is 85 dB, and back-lobe gain is -10 dB.

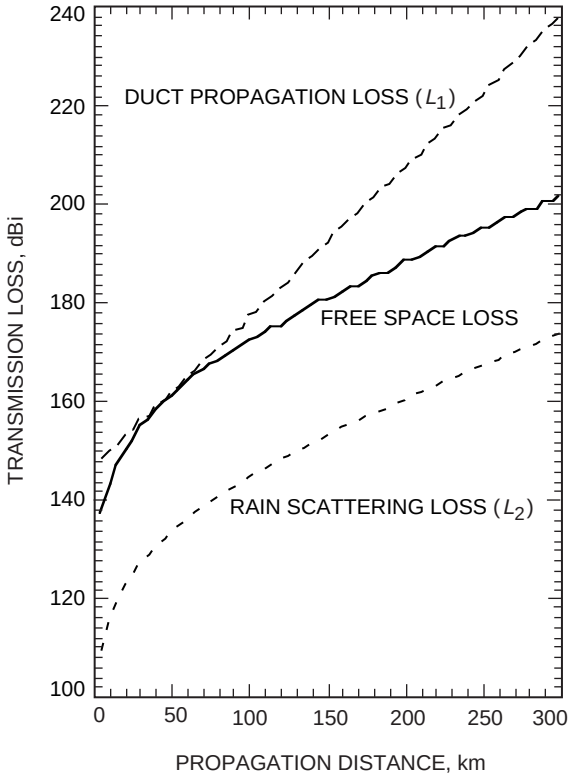

Fig. 5. A comparison of transmission losses due to ducting and rain scattering as a function of propagation distances for 0.001 percent of time in weather exceeded.

III. Worst-Case Estimate

Prior to calculating the aggregate interference power from a multitransmitter distribution in a large area, a worst-case estimate of interference effect from a single transmitter at Los Angeles on the Goldstone DSN receiver was performed. It was assumed here that the transmitter's main beam points in the direction of the DSN tracking station, while the receiver antenna may be pointing its main beam or back lobe toward the transmitter. The power received at Goldstone and the relative threshold margins were calculated based on the following parameters: for the transmitter, $P_t = -60$ dBW/Hz, with $G_t = 46$ dB (maximum gain) and the back lobe -12.5 dB; for the distance, $d = 200$ km from Los Angeles, with a percentage of time of $p = 0.001$ percent; and for the receiver, $G_r = 85$ dB (maximum gain), with a back lobe of -10 dB and a threshold of $P_{th} = -217$ dBW/Hz.

The results from a transmitter located at Los Angeles for various propagation mechanisms are listed in Table 2. Negative margins in the tables indicate that the protection-level criterion is exceeded. It was found that, when the receiver's main beam points to the transmitter,[2] its threshold is easily exceeded except for in the rain-scattering case. When its antenna back lobe points toward the interfering transmitter, there are only small positive margins for ducting and rain-scattering propagation.

We also made worst-case interference estimates for some nearby cites around the DSN antenna. The results are listed in Table 3. Since the cities have distances less than 200 km from Goldstone, all the received interference powers exceed the threshold level, regardless of whether the receiver points its main

[2] Actually, this situation rarely occurs, since the DSN antenna points above the horizon angles most of the time.

beam or back lobe towards the interfering transmitter. Thus, for a single interfering transmitter, we can conclude that, if its main beam points to the DSN antenna and if its distance from the receiver is less than 200 km, it can create a serious interference problem at the DSN receiver, causing severe spectrum degradation.

Table 2. The worst-case estimate of the interference effect from a single transmitter in Los Angeles on the Goldstone DSN receiver through various propagation mechanisms.

Propagation mechanism	EIRP, dB	Loss, dB	EIRP minus loss, dB	P_r		Margin ($P_{th} - P_r$)	
				Back lobe, dBW/Hz	Main lobe, dBW/Hz	Back lobe, dBW/Hz	Main lobe, dBW/Hz
Line of sight	−14	188	−202	−212	−117	−5	−100
Diffraction	−14	221	−235	−245	−160	28	−57
Ducting	−14	208	−222	−232	−147	15	−70
Rain scattering	−14	206	−220	−220	−220	3	3

Table 3. The worst-case estimate of the interference effect from a single transmitter at nearby cities on the Goldstone DSN receiver through various propagation mechanisms.

City	Distance from Goldstone, km	EIRP, dBW/Hz	Line of sight, dB	Diffraction, dB	Ducting, dB	Rain scattering, dB	Margin ($P_{th} - P_r$)	
							Back lobe (rain), dBW/Hz	Main lobe (ducting) dBW/Hz
Barstow	50	−14	161	163	162	133	−69	−126
Victorville	65	−14	165	169	166	137	−66	−122
Lancaster	150	−14	180	193	192	153	−50	−96
Palmdale	160	−14	183	198	197	154	−49	−91

IV. Monte Carlo Simulation

An effective way to evaluate the interference effects from an HDFS deployment on a DSN receiver is to simulate a real HDFS transmitter spatial distribution [25]. A Monte Carlo approach was used to simulate the location of each transmitter and the orientation of its antenna. Three independent random variables representing the HDFS transmitter's two-dimensional location and azimuthal antenna orientation have been selected in this simulation. It was assumed that HDFS transmitters will be randomly distributed in a circular area with various maximum radial distances, ρ_0, around an urban center. With each simulation run, each HDFS transmitter is located at a radial distance, ρ_i, from the urban center and azimuthal angle, ϕ_i, from the east, in a polar coordinate system. Figure 6 shows the geometry of the HDFS transmitter distributions and the simulation variables, where r_i is the distance from the ith transmitter to the Goldstone station, while R is the distance (equal to 200 km) from the urban center to the station. These two random variables have the following ranges:

$$0 \leq \rho_i \leq \rho_0$$

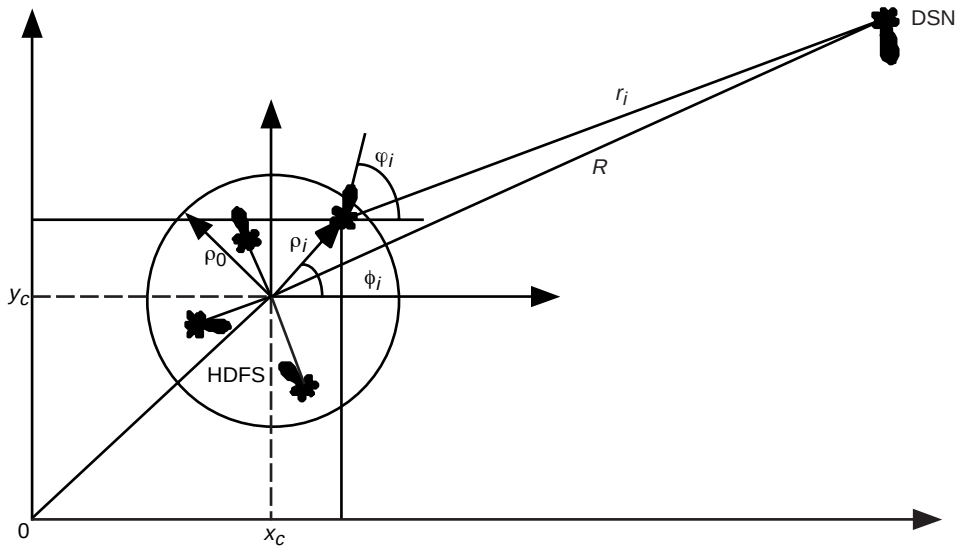

Fig. 6. HDFS spatial distribution configuration and simulation variables. Transmitters are deployed in a circular area with a maximum radius, ρ_0, around the center of Los Angeles. Each transmitter has a random location, (ρ_i, ϕ_i), and a main-beam orientation, φ_i. The Goldstone DSN receiver has a distance r_i from the receiver and a 200-km distance from the city center.

$$-180 \text{ deg} \leq \phi_i \leq 180 \text{ deg}$$

The main beam of the transmitter antenna gain has a fixed elevation angle, $\theta = 0$ deg, and a random azimuthal angle, φ, with

$$-180 \text{ deg} \leq \varphi_i \leq 180 \text{ deg}$$

Assuming that the Los Angeles metropolitan center has a geographic coordinate (x_c, y_c), the transmitter's location may be described as in a Cartesian coordinate system:

$$\left.\begin{aligned} \mathbf{X_i} &= \mathbf{x_i} + x_c \\ \mathbf{Y_i} &= \mathbf{y_i} + y_c \end{aligned}\right\} \tag{17}$$

where

$$\left.\begin{aligned} \mathbf{x_i} &= \rho_i \cos\phi_i \\ \mathbf{y_i} &= \rho_i \sin\phi_i \end{aligned}\right\} \tag{18}$$

Considering only the ducting propagation loss, L_1, with a time percent of $p = 0.001$, the total interference power spectral flux density, P_{SFD}, can be obtained by non-coherently summing all received powers at Goldstone:

$$P_{SFD} = \sum_{i}^{n} \left(P_t + G_t(\varphi_i) - L_1(\rho_i, \phi_i) \right) \tag{19}$$

in dB, where the transmitter number is $n = 3000$ and $P_t = -60$ dBW/Hz. Each simulation was performed with a random HDFS spatial distribution configuration of 3000 transmitters in the Los Angeles area. Because every transmitter was assigned three random numbers—location, ρ_i and ϕ_i, and antenna beam azimuth orientation, φ_i—9000 independent random numbers were generated for each Monte Carlo simulator run or each HDFS deployment. An interference power value at Goldstone from each pattern is obtained by combining the signal from each transmitter as given by Eq. (19). We made 1200 trials (HDFS transmitter spatial distributions), and every trial was initiated with a different sequence of random numbers. These trials were repeated for different maximum radial distances ($\rho_0 = 1$, 10, 30, and 50 km). Finally, 1200 integrated power flux density values were obtained for each fixed HDFS maximum radial distance. Figures 7(a) through 7(c) provide some examples to show the interference power fluxes for various numbers of transmitters and radial distances.

V. Simulation Results

A Monte Carlo approach was used to simulate possible future HDFS transmitter installation patterns. Since a large number of trials were performed, the results for interference power are statistically significant. Figure 8 shows interference P_{SFD} distributions at the Goldstone site for HDFS spatial distributions with different maximum radial distances (1, 10, 30, and 50 km). Each P_{SFD} distribution curve has 1200 samples with a 1-dB power increment, as stated in the previous section. The P_{SFD} curves generally shift to higher power (to the right) with increasing radial distance. Thus, the average power flux also increases with an increasing radial distance. These P_{SFD} distributions were difficult to model due to large fluctuations in the curves. However, they are significantly different from a normal (Gaussian) distribution, indicating a nonsymmetrical distribution with a gradual tail at the low-power side.

A large number of trials should be performed in a future study to improve the accuracy of the distributions. This will lead to determination of the relationship between the aggregate P_{SFD}, the transmitter antenna gain, and the radial distances of HDFS spatial distributions. Some possible HDFS transmitter deployment patterns with less interference effects on the DSN receiver also can be simulated.

When it is assumed that the aggregate power from multiple HDFS transmitters can be reduced to an equivalent single transmitter, with $P_t = -60$ dBW/Hz, an equivalent aggregate transmitter antenna gain may be deduced. JRG 7D/9D has proposed the use of a theoretical model (normal distribution) for this calculation [9–12]. For a transmitter antenna-gain pattern as described in Subsection II.C [21], $\overline{m} = 46$ dB, where $\overline{m}$ is the mean of the antenna gains averaged over all uniformly distributed azimuthal samples. For a normal distribution [9, 10], when the probability is $p(g \geq g_0) = 50$ percent and the total transmitter number is $n = 3000$, the mean aggregate antenna gain for all transmitters is $g_0 = n\overline{m} = 55$ dB.

In order to make a comparison of the aggregate antenna gain of an equivalent single transmitter determined from a normal distribution with an actual HDFS distribution, we also have derived the transmitter antenna gain from the simulation. Since an actual HDFS transmitter deployment pattern in the Los Angeles area cannot be known until it is built, an average power flux (the mean values in Fig. 8) is used for the calculation of the aggregate transmitter antenna gain. At first, the aggregate interference power spectral flux density, P_{SFD}, at Goldstone as calculated from Eq. (19) is used to infer the equivalent EIRP by $(P_{SFD} + L_1)$. For the Los Angeles–Goldstone case, $d = 200$ km and $L_1 = 208$ dB. Then, using $EIRP - P_t$, we can obtain the equivalent aggregate transmitter antenna gain, G_0. The results for different HDFS distribution radial distances are listed in Table 4.

The g_0 value determined from the normal distribution was found to approach the equivalent transmitter antenna gain, $G_0 = 55.5$ dB, calculated from the simulation, when the radial distance was $\rho_0 = 1$ km.

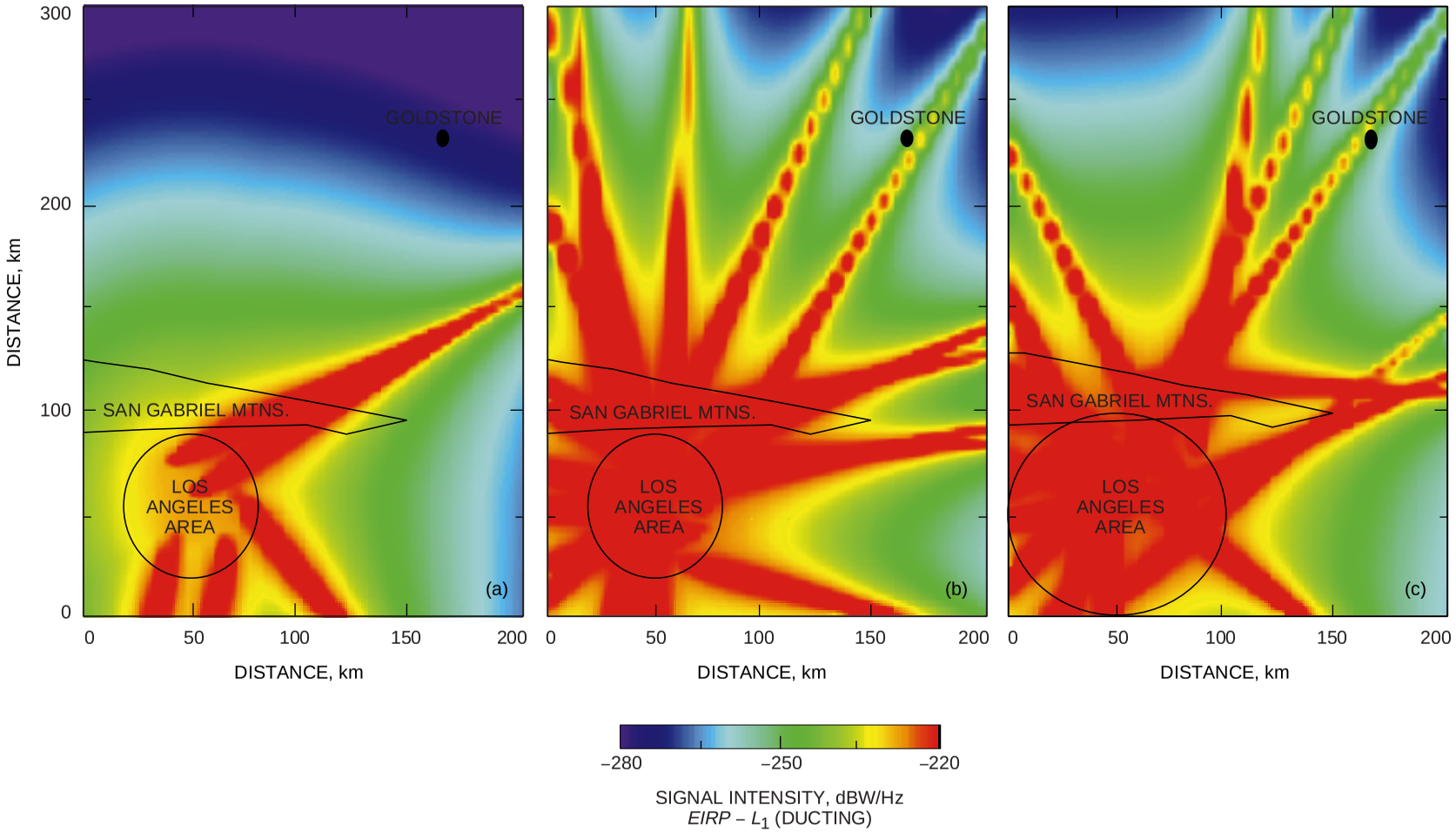

Fig. 7. The interference signal intensities for various numbers of transmitters from the Los Angeles area and an extended radius: (a) 5 transmitters with a 30-km radius, (b) 20 transmitters with a 30-km radius, and (c) 20 transmitters with a 50-km radius. The Goldstone DSN receiver is at the upper-right corner.

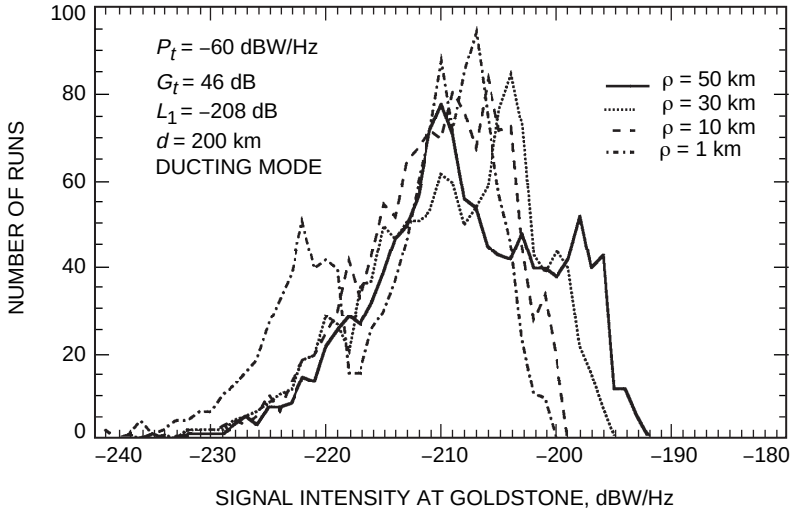

Fig. 8. Interference signal intensities at Goldstone for different HDFS extended radii. Each curve shows the signal intensity distribution from 1200 HDFS deployment patterns. Only ducting transmission loss over a 200-km distance is considered here. In general, when the HDFS extended radius increases, the signal intensities shift to higher values.

Table 4. Monte Carlo simulation results for average interference power flux density at Goldstone from 3000 transmitters in Los Angeles with different maximum radial distances.

Maximum radial distance, km	Goldstone average power flux P_{SFD}, dBW/Hz	Aggregate EIRP ($P_{SFD} + L_1$) dBW/Hz	Equivalent antenna gain G_0 ($EIRP - P_t$), dB	Margin ($P_{th} - P_r$)	
				Back lobe, dBW/Hz	Main lobe, dBW/Hz
1	−212.5	−4.5	55.5	5.5	−89.5
10	−211.5	−3.5	56.5	4.5	−90.5
30	−209.0	−1.0	59.0	2.0	−93.0
50	−205.0	−3.0	63.0	−2.0	−97.0

When the maximum radial distance of the HDFS distribution becomes large, the aggregate transmitter antenna gain calculated from an HDFS spatial distribution increases rapidly. For example, when $\rho_0 =$ 50 km, the aggregate antenna gain is $G_0 = 63$ dB for $p = 50$ percent from the simulation, which is much larger than the g_0 from a normal distribution. In this situation (a 50-km radius and a 200-km central distance), the nearest transmitter can be as near as 150 km to the receiver. If this transmitter happens to point its main beam to the receiver, then the worst case that was estimated in Section III will be exceeded. For a case of $p(g \geq g_0) < 0.1$ percent (a smaller cumulative probability), the g_0 from a normal distribution will have much smaller value than the G_0 obtained from the simulation. This suggests that, when compared with a simulated HDFS transmitter distribution, a theoretical model with an equivalent single transmitter assumption underestimates the aggregate antenna gain.

Figure 9 shows the final received interference power, P_r (DSN receiver input), for different HDFS radial distances. These results are obtained by combining the integrated average P_{SFD} with the receiver antenna azimuthal gain, G_r. The interference signals are reduced by 10 dB in the receiver antenna back lobe and increased by 85 dB at the bore site. Comparing this with the interference threshold (−217 dBW/Hz) of

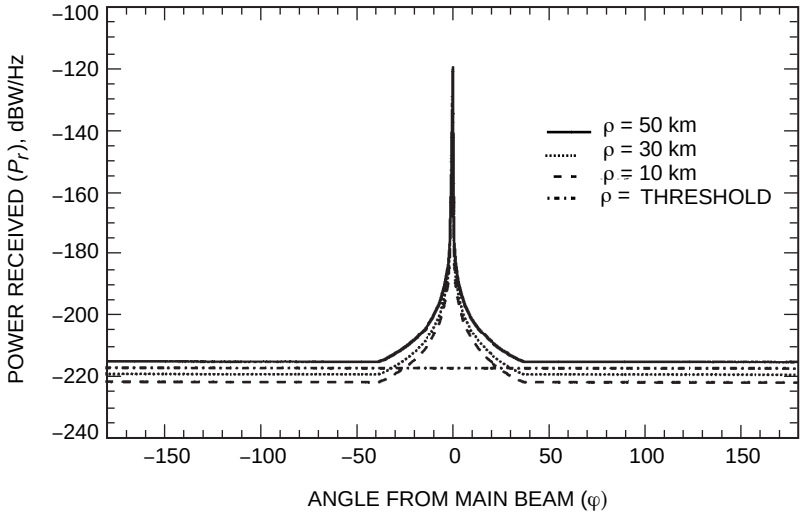

Fig. 9. Received interference powers at Goldstone after the DSN receiver antenna gain in all azimuthal angles. Three curves correspond to signals from transmitters with different extended radii. As a reference, the DSN reciever threshold level also is shown. When the radius is greater than 30 km, the threshold is exceeded.

the DSN receiver, all signals in the main lobe greatly exceed the threshold. In the back-lobe side, when the HDFS maximum radial distance is less than 50 km, only small positive margins can be expected. However, if the maximum aggregate P_{SFD} (values in the higher-power side in Fig. 8) are selected with a lower probability, both the aggregate antenna gain and the received power increase by ∼20 dB. The receiver's threshold definitely will be exceeded at all azimuthal angles.

VI. Conclusion and Summary

In this article, an approach was developed to quantitatively estimate, using a Monte Carlo simulation, the aggregate interference power from various transmitter deployment patterns with random orientations. We have estimated the interference level of the HDFS from the Los Angeles area at the Goldstone 70-m DSN tracking station. Based on our results, we find that the HDFS will become a serious problem for the DSN tracking-station receivers, especially when the HDFS transmitter main beams are directly pointed to the DSN antenna. In addition, if HDFS transmitters operate with higher transmitter power or at distances less than 200 km from the DSN antenna, the receiver's performance may be severely degraded. We summarize these results in the following.

(1) A thorough literature search was conducted for all ITU documents related to transhorizon propagation interference effects and all HDFS operating parameters. Interference from a single transmitter through ducting, rain scattering, and diffraction has been fully investigated. Aggregate interference effects from HDFS transmitter spatial distributions have been assessed using a simulation technique for the first time.

(2) Worst-case estimates were performed for a single transmitter with the highest power level in the Los Angeles area and the cities near Goldstone. At a 200-km separation distance, when the transmitter's main beam is exactly pointed at the DSN antenna, only small positive margins can be expected relative to the back lobe of the receiver antenna for 0.001 percent of the time (weather condition). For some cities with distances less than 200 km, interference signals will largely exceed the threshold of the receiver.

(3) Monte Carlo simulations were conducted to examine the interference effects on the Goldstone tracking station using 3000 HDFS transmitters in the Los Angeles area. The impact of HDFS EIRP levels, spatial distributions, and maximum radial distances has been examined. Preliminary statistical results for aggregate power distributions from 1200 trials with different maximum radial distances of the HDFS distributions were obtained. The results show that, when the HDFS transmitter spatial distributions have large radial distances, aggregate transmitter antenna gains and interference power received at Goldstone are much greater than those calculated from a normal distribution. When the radial distance is 50 km, the DSN receiver interference threshold will be exceeded.

(4) We have developed an approach, using a Monte Carlo simulation, to quantitatively study the interference effect of HDFS transmitters with various orientations and distributions on the DSN. As a future study, actual HDFS distributions can be simulated more realistically, and any HDFS deployment patterns proposed to mitigate the interference effects, such as coordinated (planned) antenna pointing, can be examined using this simulation tool. This tool also can be used to estimate potential interference to the DSN from other transhorizon terrestrial services.

Acknowledgments

We would like to thank Dr. Anil V. Kantak for reviewing this article and Dr. Nasser Golshan for his suggestions. We also are grateful to Dr. Dan Bathker of JPL TMOD and to Dr. Louis J. Ippolito of Stanford Telecom ACS for his input.

References

[1] "Elements of a Methodology to Estimate the Global Distribution of Potential Hub Stations of Point-to-Multipoint Fixed Service Systems," contributed by USA, Document 7D-9D/36-E, ITU-R, 1998.

[2] "Correspondence Group on High Density Systems in the Fixed Service (HDFS) Above 30 GHz," Resolutions 126, 726, and 133 (WRC-97), Document 9B/66-E, 7D-9D/32, ITU-R, 1998.

[3] "Prediction Procedure for the Evaluation of Microwave Interference Between Stations on the Surface of the Earth at Frequencies Above About 0.7 GHz," Recommendation ITU-R P.452-8, ITU-R, 1997.

[4] "Method for the Determination of the Coordination Area Around an Earth Station in Frequency Band Between 1 GHz and 40 GHz Shared Between Space and Terrestrial Radio Communication Services," Appendix S7 (28), Radio Regulations, ITU-R, 1994.

[5] "A Comparison of Coordination Distances for Propagation Mode (1) of Appendix S7 Calculated Using Recommendation ITU-R P.620-3 and Recommendation ITU-R IS.847-1, and Data Measured in Europe for Frequencies Between 6 and 30 GHz," contributed by UK, Document 3M/25-E, ITU-R, 1998.

[6] "Determination of the Coordination Area of an Earth Station Operating With a Geostationary Space Station and Using the Same Frequency Band as a System in a Terrestrial Service," Recommendation ITU-R IS.847-1, ITU-R, 1993.

[7] "Propagation Data Required for the Evaluation of Coordination Distances in the Frequency Range 0.85–60 GHz," Recommendation ITU-R P.620-3, ITU-R, 1997.

[8] CCIR, "Propagation Data Required for the Evaluation of Coordination Distance in the Frequency Range 1–40 GHz," Report 724-2, in vol. V, *Propagation in Non-Ionized Media*, Recommendations and Reports of the CCIR, 1986, Geneva: Intl. Telecomm. Union, 1986.

[9] "Consideration of the Statistical Characteristics of Parameters Affecting Sharing Between Stations in the Space Research Service and HDFS Stations in the Fixed Service in Bands Above 30 GHz," contributed by USA, Document US7D-9D/xxx, ITU-R, 1998.

[10] "Methodology to Estimate the Number of Stations and to Aggregate the Emissions of High-Density Fixed Systems in the Fixed Service for the Purpose of Determining the Coordination Contour and Coordination Distance in Bands Above 30 GHz Shared with Receiving Earth Stations in the Space Research Service," contributed by USA, Document USJRG 7D-9D/xyz, ITU-R, 1999.

[11] "Co-Frequency Sharing of Spectrum Between High-Density Fixed Systems and Space Research Systems in the 31.8–32.3 GHz Band," contributed by Canada, Document 7D-9D/31-E, ITU-R, 1998.

[12] "Co-Frequency Sharing of Spectrum Between High-Density Fixed Systems and Scientific Satellite Systems in the 37–38 GHz and 40.0–40.5 GHz Bands," contributed by Canada, Document 7D-9D/39-E, ITU-R, 1998.

[13] CCIR, "Radiometeorological Data," Report 563-3, in vol. V, *Propagation in Non-Ionized Media*, Recommendations and Reports of the CCIR, 1986, Geneva: Intl. Telecomm. Union, 1986.

[14] CCIR, "Effects of Tropospheric Refraction on Radiowave Propagation," Report 718-2, in vol. V, *Propagation in Non-Ionized Media*, Recommendations and Reports of the CCIR, 1886, Geneva: Intl. Telecomm. Union, 1986.

[15] B. R. Bean and E. J. Dutton, *Radio Meteorology*, New York: Dover Publications Inc., 1966.

[16] "Propagation by Diffraction," Recommendation ITU-R P.526-5, ITU-R, 1997.

[17] R. K. Crane, "Bistatic Scatter From Rain," *IEEE Trans. Ant. Prop.*, vol. AP-22, pp. 312–320, 1974.

[18] J. Awaka, K. Nakamura, and H. Inomata, "Bistatic Rain-Scatter Experiment at 34.8 GHz," *IEEE Trans. Ant. Prop.*, vol. AP-31, pp. 693–698, 1983.

[19] M. P. M. Hall, editor, *Effects of the Troposphere on Radio Communication*, London: Peter Peregrinus, 1980.

[20] R. K. Crane, "A Review of Transhorizon Propagation Phenomena," *Radio Sci.*, vol. 16, pp. 649–669, 1981.

[21] "Mathematical Model of Average Radiation Patterns for Line-of-Sight Point-to-Point Radio-Relay System Antennas for Use in Certain Coordination Studies and Interference Assessment in the Frequency Range From 1 to About 40 GHz," Recommendation ITU-R F.1245, ITU-R, 1997.

[22] CCIR, "Attenuation by Atmospheric Gases," Report 719-2, in vol. V, *Propagation in Non-Ionized Media*, Recommendations and Reports of the CCIR, 1886, Geneva: Intl. Telecomm. Union, 1986.

[23] CCIR, "Scattering by Precipitation," Report 882-1, in vol. V, *Propagation in Non-Ionized Media*, Recommendations and Reports of the CCIR, 1886, Geneva: Intl. Telecomm. Union, 1986.

[24] *Radio Regulations 3*, Appendices 25–44, Norwegian Telecommunications Administration, Oslo, 1982.

[25] "Principles and a Methodology for Frequency Sharing in the 1610.6–1613.8 and 1660–1660.5 MHz Bands Between the Mobile-Satellite Service (Earth-to-Space) and the Radio Astronomy Service," contributed by Radiocommunication Study Group 8, Document 8/1021-E, ITU-R M., ITU-R, 1997.